



Palynofacies, Organic Petrography, and Source Rock Potential of the Toarcian Quse Formation Oil Shale in the Tibetan Tethys, China

Ahmed Mansour, Thomas Gentzis, Guoqing Xia, Humberto Carvajal-Ortiz, Seare Ocubalidet, Haisheng Yi, and Haytham El Atfy 

Abstract

The southern Qiangtang Basin located in the central Tibetan Plateau of the eastern Tethys is among the most significant petroliferous provinces in China. In this chapter, lower Toarcian sediments represented by thick oil shale succession from the Bilong co area, were studied. Geochemical screening, organic petrographic, and palynological analyses were conducted to investigate kerogen characteristics, thermal maturity, and depositional environment. The Quse and Sewa formations of the study section were divided into two groups according to time of deposition and geochemical features. The first group is represented by the early Toarcian interval and deposited during prevalent anoxia with excellent organic matter richness and hydrocarbon generation potential of kerogen Type II. Amorphous organic matter (AOM) is the foremost constituent compared to the low phytoclast content. The anoxic interval of this group is consistent with the early Toarcian oceanic anoxic event (T-OAE). The second group of the upper Bajocian-Bathonian interval refers to the Sewa Formation, which is dominated by good to very good organic matter deposited

predominantly in a dysoxic environment. Organic matter comprised varied kerogen types, including IV, III, II/III, and II, and has hydrocarbon potential that varies from poor to very good. However, the majority of samples from both groups are still in the early stage of the oil window. Paleoenvironmental conditions were variable from brackish shallow marine to distal inner-neritic shelf with enhanced organic matter preservation.

Keywords

Kerogen • Kerogen quantity • Thermal maturity • Qiangtang Basin • Toarcian anoxia

1 Introduction

The oceanic anoxic event that occurred during the Toarcian stage of the Early Jurassic period (T-OAE, *ca.* 183 Ma) was responsible for substantial global depositions of organic-rich sediments (Jenkyns, 2010). This is evidenced by the regional distribution of marker marine taxa, such as ammonites and nannofossils (Chen et al., 2018; Yi et al., 2003), which undoubtedly confirm a global context of a synchronous anoxic event. The Toarcian is marked by the large-scale occurrence of petroleum-bearing basins of organic matter-rich black shale and limestone, particularly in China (Chen et al., 2005; Fu et al., 2014; Ji et al., 2014; Xia et al., 2017; Yi et al., 2013). Many of the previous works have focused on the Toarcian in the eastern Tethys Tibetan Plateau employing various approaches from macro- and micro-paleontology, paleomagnetism (e.g., Ding et al., 2013; Ma et al., 2017; Wang et al., 1997, 2019), and organic petrography as well as organic geochemistry (e.g., Chen et al., 2005; Fu et al., 2014; Ji et al., 2014; Xia et al., 2017; Yi et al., 2013). However, palynofacies analysis, organic maceral composition, and organic geochemistry investigations of the upper Quse Formation in southern Qiangtang

A. Mansour
Geology Department, Faculty of Science, Minia University,
Minia, 61519, Egypt

T. Gentzis · H. Carvajal-Ortiz · S. Ocubalidet
Core Laboratories, 6316 Windfern Road, Houston,
TX 77040, USA

G. Xia · H. Yi
State Key Laboratory of Oil and Gas Reservoir Geology
and Exploitation, Chengdu University of Technology,
Chengdu, 610059, China

H. El Atfy (✉)
Department of Geosciences, University of Tübingen,
72076 Tübingen, Germany
e-mail: el-atfy@daad-alumni.de

Geology Department, Faculty of Science, Mansoura University,
Mansoura, 35516, Egypt

Basin are absent. The southern Qiangtang Basin is a giant sedimentary archive in central Tibet, which contains a well-preserved outcrop section of organic-rich Toarcian deposits (Fu et al., 2014, 2017; Yi et al., 2003). Thus, the studied basin offers a good chance to assess potential source rocks and elucidate the environment of deposition that controlled the accumulation of organic matter (OM) in the Bilong co section.

The present work focuses on the potential intervals within the topmost part of the Quse Formation in the Bilong co section that could infer source rock. Here, we present an integrated multi-proxy approach comprised of TOC, Rock-Eval pyrolysis, organic and inorganic sulfur content, organic petrography, maceral characterization, and palynofacies to investigate kerogen quantity, quality, hydrocarbon generation potential, and thermal maturity. Although this study aimed to define source rock characteristics of the organic-rich Quse Formation, palynofacies analysis provides a reliable indicator to develop a more holistic evaluation of the prevalent environment in terms of depositional settings, type, and origin of kerogen, and oxygen regime. All of these components are fully considered in this contribution and, hence, improve the limited knowledge about the less-investigated Toarcian source rock intervals and paleoenvironments of the Quse Formation, southern Qiangtang Basin.

2 Geological Settings

2.1 Structural Settings

The Qiangtang Basin covers a large area ranging from the extreme north to central parts of the Tibetan Plateau (Fig. 1a). This basin has been influenced by successive tectonic events that resulted in a tectonic jigsaw. The basin is bound by the Jinsha suture northward and the Bangong-Nujiang suture southward, which separates the Qiangtang main basinal block from the Lhasa blocks and Hoh Xil-Songpan, correspondingly (Fig. 1b; Kapp et al., 2007; Wang et al., 2014; Yin & Harrison, 2000). The main basinal block of the Qiangtang Basin (Fig. 1c) was investigated recently. Structural data showed that the block can be subdivided into the North and South Qiangtang blocks, which are detached by Longmu Co-Shuanghu Suture Zone (LSSZ) trending toward the NWW (Fang et al., 2016). The LSSZ presents the central uplift belt. The aforementioned three suture zones that bound the Qiangtang blocks were shaped as a result of the consecutive tectonic activities of the Tethys from the Permian to the Jurassic (e.g., Ding et al., 2013; Wang et al., 1997, 2019).

In the Early Permian, strong tectonic activity resulted in the separation of the main Qiangtang Basin from eastern

Gondwana (Zhu et al., 2013). This setting contributed to further subsidence of the Qiangtang Basin, which submerged under the sea as an epicontinental shelf environment (Wang et al., 2004). Subsequently, in the Late Triassic, a fast-northward drifting resulted in a strong collision with the Hoh Xil-Songpan Block, creating a syn-tectonically foreland basin to the south of the Hoh Xil-Songpan and a thrust-fold belt system along the northern edge of the Qiangtang Basin (Li et al., 2002). Since the Early Jurassic, the paleogeographic position of the Qiangtang basinal block was at mid-paleolatitudes in the northeastern portion of the Tethys, where a hemipelagic shelf to open-ocean marine circumstances prevailed (Wang et al., 2004). This was followed by a westward collision up to the Early Cretaceous between the Qiangtang Basin and the Lhasa Block, creating yet another syn-tectonic thrust-fold and foreland basin over the Bangong-Nujiang suture. Additionally, these settings triggered a consequent closing of the Meso-Tethys due to a westward retreat of the Qiangtang Basin and thus, the termination of the Jurassic seaway that was followed by strong uplifting and erosion of the adjoining areas (Li et al., 2002; Sengör, 1987). The consecutive activity of subduction at the oceanic plate margins of the Neo-Tethys along with strong collisions of the Neo-Tethyan arcs and India with the Lhasa High did not result in tectonic configuration changes of the Qiangtang, but only minor intra-block basins were developed and have been filled with erosional red beds at sutures and fault zones during periods of active tectonic uplift, which resulted in shaping the Qiangtang Basin to its present position (Fang et al., 2016).

2.2 Stratigraphic Framework

The surface outcrop of the southern Qiangtang Basin contains a thick stratigraphic section that averages more than 5000 m in thickness. The southern Qiangtang Basin includes marine strata that represent, from older to younger, the Lower Jurassic Quse, Middle Jurassic Sewa, Buqu, Xiali, and the Upper Jurassic Suowa formations, which are synchronous to the equivalent rock units in the adjoining northern Qiangtang Basin (Chen et al., 2018; Ding et al., 2013; Li, 2016; Ma et al., 2017; Wang et al., 1997, 2019). The Toarcian strata are thought to be represented in the Quse Formation, which overlies the Triassic shale and limestone (Fig. 2). This is based on age-diagnostic ammonites of a typical Early Jurassic, including *Schlotheimiidae* sp. and *Hildoceratacaea* sp. (Su et al., 2015; Yi et al., 2003). The upper interval of the Quse Formation comprises black limestone and oil shale along with thick marl and calcareous mudstone (Fig. 3). The OM-rich shale and limestone are restricted only to the Quse and Sewa rock units within the Bilong co region (Fig. 2).

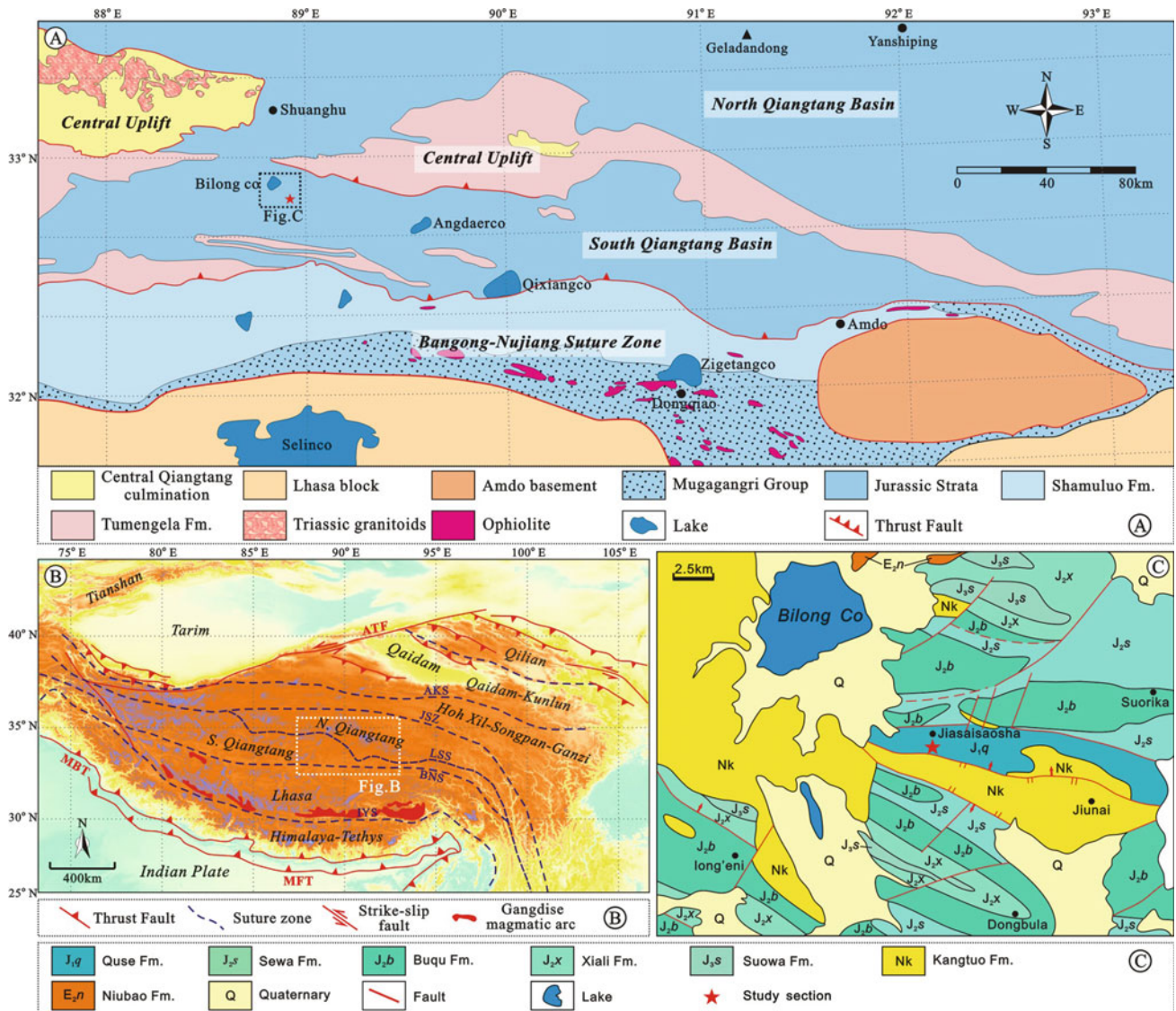


Fig. 1 (a) Geological map of the Qiangtang basin (modified after Ma et al., 2017) showing the Bilong co area. (b) Tectonic map of the Tibetan Plateau showing the southern Qiangtang Basin and adjacent regions, ATF = Altyn Tagh Fault, AKS = Anemaqen-Kunlun Suture, JSZ = Jinsha Suture Zone, LSS = Longmu Co-Shuanghu Suture, BNS = Bangong-Nujiang Suture, IYS = Indus-Yarlung Suture, MFT = Main Front Thrust, and MBT = Main Boundary Thrust. (c) Simplified geological map of the Bilongco region in the southern Qiangtang basin and location of the study section (modified from Wang et al., 2012)

The Bajocian-Bathonian Sewa Formation overlies the Quse Formation and consisted of limestone, gray marl, and mudstone facies (Yin & Chandler, 2016). The Buqu Formation is dominated by carbonate platforms rich in brachiopods *Holcothyris-Burmhirhynchia*, which are diagnostic of the late Bathonian age (Yao et al., 2011). The Callovian Xiali Formation comprised mainly fine-to coarse-grained sandstone. The Suowa Formation was formed during the Oxfordian-Kimmeridgian and is composed of shallow marine limestone with minor intercalations of black-gray calcareous mudstone and marlstone (Chen et al., 2018; Ma et al., 2017; Yao et al., 2011; Yi et al., 2005).

3 Material and Methods

The present study integrates organic petrographic and geochemical screening along with palynofacies analysis to qualitatively and quantitatively assess the hydrocarbon source potential of the Quse and Sewa formations. For this purpose, a number of 22 samples were collected from an outcrop section in the Bilong co, southern Qiangtang Basin, Tibet Plateau (Figs. 1, 2). All samples were tested for palynofacies analysis, random vitrinite reflectance (%VR_{o,r}), as well as TOC and Rock-Eval® pyrolysis.



Fig. 2 (a–d) Field photographs from the Bilong co area in the southern Qiangtang Basin illustrate the oil shales, marl, and limestone lithofacies

3.1 Elemental Composition, Organic Carbon, and Rock–Eval® Pyrolysis

Carbonate content was calculated from the measurement of CaO using bulk rock geochemistry analysis. 5 g of each powdered rock sample (*ca.* 0.074 mm) were soaked in a concentrated HNO₃ and HF acids mixture at 176–200 °C for several days. This was followed by diluting the remnant solution using deionized water to measure the major oxides (e.g., SiO₂, Al₂O₃, CaO, MgO, FeO, Na₂O, MnO, K₂O, TiO₂, and P₂O₅) using X-ray fluorescence. The analytical precision was well than $\pm 0.5\%$ with a detection limit of 0.01%. The CaCO₃ content was calculated by multiplying the CaO values by 0.7146 to convert the measured calcium oxide into Ca, and the obtained result was then multiplied by 2.4973 to get the CaCO₃ content (Table 1). Elemental analysis of (bulk) rock samples was carried out in the Analytical Laboratory, Beijing Research Institute of Uranium Geology, China National Nuclear Corporation.

Total organic carbon (TOC) and Rock–Eval® pyrolysis measurements were conducted on all samples at the Core Laboratories facilities in Houston, USA. An aliquot of *circa*

60 mg from the fine powder of each pulverized sample was analyzed by an open system programmed pyrolysis (Rock–Eval® 6) instrument (Vinci Technologies, France) using the IFP’s Bulk-Rock technique for source rocks (e.g., Behar et al., 2001; Carvajal-Ortiz & Gentzis, 2015). The pyrolysis analysis was conducted in a nitrogen atmosphere, and the free hydrocarbons were detected using a flame ionization detector. An infrared cell detected the evolved gases of CO and CO₂. During pyrolysis, samples were heated to 300 °C and stayed isothermally for 3 min, followed by a temperature increase to 650 °C with a steady rate of 25 °C/min. Pyrolysis was followed by oxidation that took place in an isolated oven. Rock–Eval pyrolysis provides a group of essential parameters, including TOC (wt%), S₁ (free hydrocarbons produced without cracking of kerogen, in mg HC/g rock), S₂ (thermally-cracked hydrocarbons at pyrolysis temperatures of 300–600 °C, same units as S₁), S₃ (released CO and CO₂ due to thermal cracking of kerogen, in mg CO₂/g rock), S₄ (residual carbon content, mg C/g rock), and S₅ (mineral carbon and can be used to calculate carbonate content of samples, mg CO₂/g rock), and T_{max} (the temperature at which maximum hydrocarbon released (S₂))

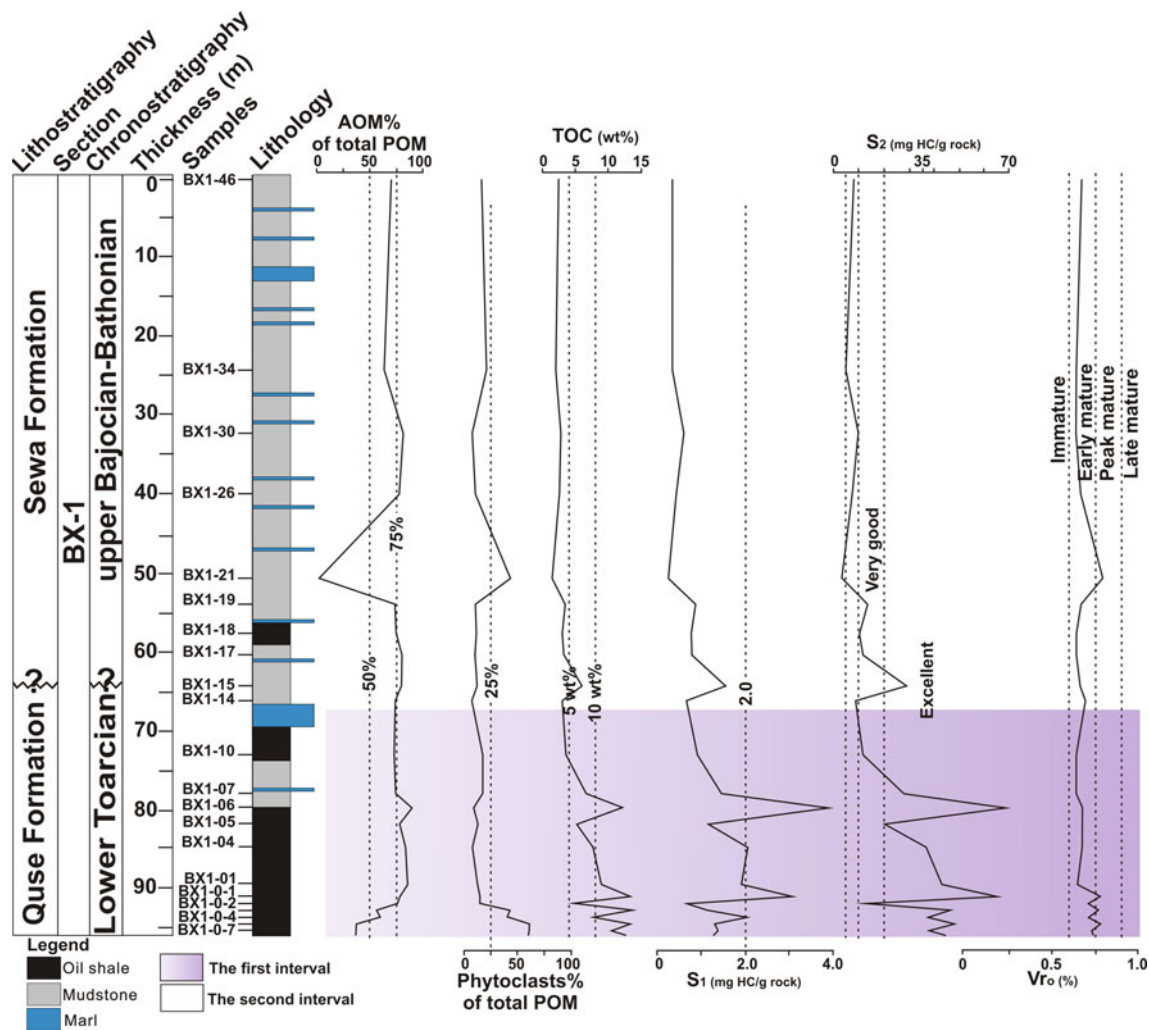


Fig. 3 Stratigraphic distribution of the TOC/Rock–Eval pyrolysis parameters, vitrinite reflectance, as well as AOM and phytoclast contents from the upper part of the Quse Formation in the Bilong co section

during kerogen cracking, °C). Parameters such as hydrogen index ($HI = (S_2/TOC) \times 100$, mg HC/g TOC), oxygen index ($OI = (S_3/TOC) \times 100$, mg CO₂/g TOC), and production index [$PI = S_1/(S_1 + S_2)$] were deduced from the above-mentioned readings.

3.2 Sulfur Analysis

The organic sulfur proportions bounded in sedimentary OM significantly impact the source rock kinetics and consequently, thermal maturity of OM. Thus, Rock–Eval 7S® was employed to quantify the total sulfur (TS, organic, and inorganic) and to identify and quantify the sulfur species in five samples selected based on the highest TOC and S₂ contents. Rock–Eval 7S® has an additional oven, where sulfur compounds are converted into SO₂ at 900–1200 °C. SO₂ released during pyrolysis and oxidization is detected and measured in real time by a UV detector, followed by calculation of various

parameters, including S₁ S_{org}, S₂ S_{org}, residual sulfur, retained sulfur, and sulfate sulfur as well as pyritic sulfur. The basic/total sulfur IFP methodology was utilized to implement the sulfur speciation analysis. The temperature program is alike to the Basic/Bulk–Rock method that is widely applicable for source rocks exploration. It initiates at 300 °C and retains isothermally for 3 min., followed by a gradual increase of 25 °C/min. ramp until 650 °C, but with a prolonged analysis period throughout the oxidation phase (with a 20 °C/min ramp from 300 °C to 1200 °C for the complete decay of sulfate moieties). For further particulars of sulfur measurements, see Lamoureux-Var et al. (2019).

3.3 Organic Petrography

All samples collected from the Quse and Sewa formations were prepared for organic petrography using the whole-rock method and crushed into ca. 840 μm (–20 mesh) and

Table 1 Organic geochemical data of TOC/Rock–Eval Pyrolysis and vitrinite reflectance along with distribution of POM composition throughout the studied succession of the Quse Formation from the southern Qiangtang Basin

| Sample | CaCO ₃ (%) | TOC (wt %) | S _{total} (wt %) | S ₁ (mg HC/g rock) | S ₂ (mg HC/g rock) | S ₃ (mg HC/g CO ₂) | T _{max} (°C) | V _{Ro} (%) | HI | OI | PI | AOM | Palynomorphs | Phytoclasts | Kerogen types |
|---------|-----------------------|------------|---------------------------|-------------------------------|-------------------------------|---|-----------------------|---------------------|--------|-------|------|------|--------------|-------------|---------------|
| BX1-46 | 34.8 | 2.49 | | 0.34 | 6.91 | 0.89 | 432 | 0.67 | 277.51 | 42.97 | 0.05 | 70 | 14.8 | 15.2 | II > > I |
| BX1-34 | 31.3 | 2.02 | | 0.35 | 5.23 | 0.78 | 430 | 0.64 | 258.91 | 45.54 | 0.06 | 63.4 | 15.8 | 20.8 | II > > I |
| BX1-30 | 34.5 | 2.79 | | 0.58 | 8.96 | 0.80 | 430 | 0.64 | 321.15 | 35.48 | 0.06 | 81 | 11.8 | 7.2 | II > > I |
| BX1-26 | 28.8 | 2.51 | | 0.39 | 6.71 | 1.07 | 432 | 0.67 | 267.33 | 52.19 | 0.05 | 77 | 12.6 | 10.4 | II > > I |
| BX1-21 | 46.6 | 1.48 | | 0.22 | 2.38 | 0.61 | 439 | 0.79 | 160.81 | 43.92 | 0.08 | 3.4 | 53.6 | 43 | III > IV |
| BX1-19 | 39.2 | 3.42 | | 0.89 | 13.26 | 0.95 | 432 | 0.67 | 387.72 | 33.92 | 0.06 | 73 | 16.8 | 10.2 | II > > I |
| BX1-18 | 37.6 | 3.02 | | 0.78 | 10.69 | 0.83 | 430 | 0.64 | 353.97 | 33.77 | 0.07 | 74.6 | 14.2 | 11.2 | II > > I |
| BX1-17 | 37.9 | 3.19 | | 0.77 | 11.33 | 0.81 | 430 | 0.64 | 355.17 | 31.35 | 0.06 | 79.4 | 10.8 | 9.8 | II > > I |
| BX1-15 | 39.4 | 6.00 | | 1.55 | 28.57 | 1.28 | 431 | 0.66 | 476.17 | 27.67 | 0.05 | 80.2 | 7.6 | 12.2 | II ≥ I |
| BX1-14 | 28.1 | 2.96 | | 0.66 | 8.66 | 1.01 | 433 | 0.69 | 292.57 | 38.85 | 0.07 | 73.8 | 19.2 | 7 | II > > I |
| BX1-10 | 34.7 | 3.53 | | 0.91 | 11.62 | 1.00 | 430 | 0.64 | 329.18 | 32.01 | 0.07 | 72.6 | 10 | 17.4 | II > > I |
| BX1-07 | 22.1 | 6.72 | | 1.45 | 28.12 | 1.78 | 430 | 0.64 | 418.45 | 34.08 | 0.05 | 74.2 | 8.8 | 17 | II ≥ I |
| BX1-06 | 33.5 | 12.21 | 0.92 | 3.88 | 68.53 | 1.52 | 432 | 0.67 | 561.26 | 17.12 | 0.05 | 89.2 | 2.2 | 8.6 | II ≥ I |
| BX1-05 | 25.4 | 5.19 | | 1.15 | 20.02 | 1.19 | 432 | 0.67 | 385.74 | 25.82 | 0.05 | 78 | 9.4 | 12.6 | II ≥ I |
| BX1-04 | 29.9 | 7.78 | | 2.04 | 36.68 | 1.32 | 432 | 0.67 | 471.47 | 22.24 | 0.05 | 83.2 | 9.2 | 7.6 | II ≥ I |
| BX1-01 | 16.2 | 9.01 | 0.53 | 1.91 | 42.49 | 2.20 | 430 | 0.64 | 471.59 | 32.08 | 0.04 | 85 | 3 | 12 | II ≥ I |
| BX1-0-1 | 22.3 | 13.48 | 0.68 | 3.06 | 64.9 | 2.23 | 438 | 0.78 | 481.45 | 21.44 | 0.05 | 78 | 7.2 | 14.8 | II ≥ I |
| BX1-0-2 | 24.0 | 4.75 | | 0.63 | 12.93 | 1.93 | 434 | 0.71 | 272.21 | 45.05 | 0.05 | 75.6 | 10 | 14.4 | II > > I |
| BX1-0-3 | 23.8 | 13.81 | | 1.13 | 46.1 | 4.87 | 437 | 0.76 | 333.82 | 44.82 | 0.02 | 56.2 | 1.6 | 42.2 | II |
| BX1-0-4 | 32.9 | 7.87 | | 2.04 | 37.83 | 1.29 | 434 | 0.71 | 480.69 | 18.30 | 0.05 | 59.6 | 0.6 | 39.8 | II |
| BX1-0-6 | 31.3 | 13.48 | 0.62 | 1.32 | 47.73 | 4.05 | 438 | 0.78 | 354.08 | 38.65 | 0.03 | 37.4 | 2 | 60.6 | II |
| BX1-0-7 | 45.5 | 10.54 | 0.92 | 1.35 | 38.04 | 2.67 | 435 | 0.73 | 360.91 | 34.44 | 0.03 | 36.8 | 3.2 | 60 | II |

homogenized in an epoxy plug using an Epo-Thin epoxy resin and hardener (2:1 per unit volume). The epoxy plugs were grinded using 320 μm followed by 600 μm cloths and polished by means of alumina powder (0.3 μm and 0.05 μm) and H₂O at two stages to get a relief-free surface. Vitrinite reflectance analysis was performed under an oil immersion objective of 50 × ($n_{oil} = 1.514$ at 23 °C) using the reflected light microscope Zeiss Axio Imager® A2m, which is equipped with a digital camera and UV light source. The total magnification used was 500 ×. Additionally, a conventional glass standard of 0.477% was used on primary vitrinite and bitumen to measure the random reflectance values. All preparation techniques and measurements of maceral composition and vitrinite reflectance were carried out at the Advanced Technology Center, Core Laboratories, Houston, USA. Further, information on samples investigations and maceral description can be found in ASTM D7708-14 (2014) and the ISO standards (ISO 7404-part 2, 2009; ISO 7404-part 5, 2009).

3.4 Palynofacies Preparation of Samples

The lithologic composition of samples is represented mainly by dark-olive to black calcareous mudstone and oil shale with insignificant intercalations of marl facies. Nearly, 10 g of each sample were used for palynological analysis utilizing the preparation protocol of Wood et al. (1996). Demineralization treatment includes HCl (34%) and HF (70%) acids followed by sieving of the organic residue using a nylon mesh (10 μm). Oxidative methods were avoided to introduce reliable palynofacies results. The kerogen residue was mounted onto glass slides that were then dried and coverslips were added with a drop of Canada balsam. This step produced a permanent mount with excellent optical properties for palynofacies investigations. Two slides were prepared for microscopic investigation of each sample using a transmitted light microscope (OMAX ToupView). Palynofacies preparation was carried out at the Micropaleontology and Stratigraphy Laboratory, Minia University, Egypt.

4 Results and Discussion

4.1 Kerogen Quantity and Quality

4.1.1 Geochemical Characterization

The OM quantity of the investigated succession is expressed in terms of TOC wt% (Peters & Cassa, 1994). Generally, high contents of TOC reveal high primary productivity and enhanced preservation potential during deposition at the substrate. High organic carbon content is a reliable indicator of kerogen quantity but it is insufficient to indicate source potential as a part of the TOC may be inert or reworked/recycled (Carvajal-Ortiz & Gentzis, 2015; Espitalié et al., 1985; Peters, 1986; Peters & Cassa, 1994; Rullkötter et al., 1988; Chap. 2 of this book).

In the current study, the OM richness was assessed using the TOC and Rock-Eval S_1 and S_2 parameters. The analyzed section from the Quse Formation showed a very good to excellent source potential with variable richness and quality. The upper Quse and Sewa formations are divided, based on age, into two intervals, which are the lower Toarcian as well as the upper Bajocian-Bathonian, respectively (Fig. 3). The first interval represents the lower Toarcian and is 30 m in thickness, showing a more prominent richness than the upper Bajocian-Bathonian section (Fig. 3). Besides, it is marked by oscillating TOC readings ranging from 3.5 to 13.8 wt% (avg. 9 wt%). Moreover, it has fair S_1 values varying from 0.6 to 3.9 mg HC/g rock and high S_2 content that fluctuates between 20.0 and 61.6 mg HC/g rock (Table 1, Figs. 3 and 4). The upper Bajocian-Bathonian interval of the Sewa Formation is 65 m in thickness, and encountered lower OM richness compared to the early Toarcian interval. It has good TOC content that ranges from 1.5 to 3.4 wt%, and S_2 values that vary between 2.4 and 13.3 mg HC/g rock (Table 1, Figs. 3 and

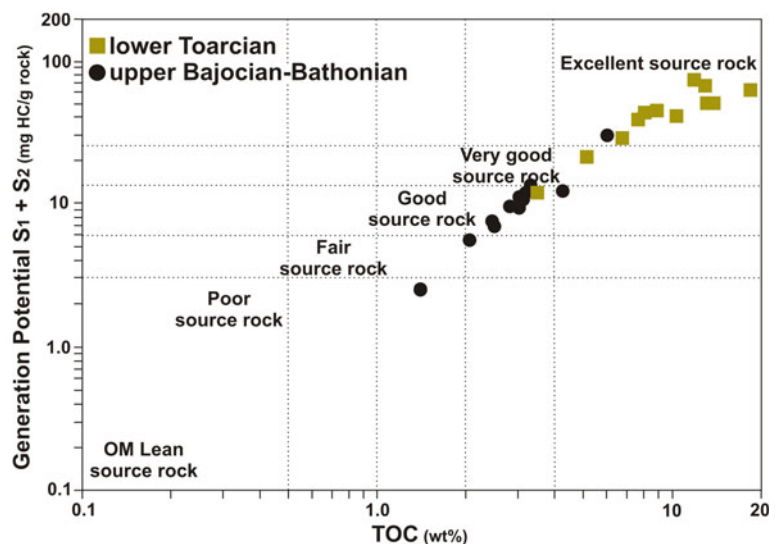
4). The lower part of the Sewa interval is more in richness. It differs in TOC and S_2 from 2.9 to 6.0 wt%, and from 8.7 to 28.6 mg HC/g rock, respectively (Table 1, Figs. 3 and 4). The previous discussion reveals that the Sewa Formation possesses good to very good source potential by means of superb generative potential in the lower part of the early Toarcian section.

Several parameters and correlations evaluate the quality and kerogen types of the studied samples. The modified van Krevelen diagram (Fig. 5) is a correlation between oxygen index (OI) and hydrogen index (HI), utilized to classify various types of kerogen. The diagram reveals that the potential source rocks of the Quse and Sewa formations contain mixed kerogen Type II/III to Type II. The early Toarcian section is dominated by kerogen Type II compared to the late Bajocian-Bathonian interval. The S_2 versus TOC correlation diagram is also used to typify kerogen in source rocks (Fig. 6). The correlation supports the conclusion from the modified van Krevelen diagram. It also elucidates homogeneous OM composition in the late Bajocian-Bathonian interval with a correlation coefficient of $r = 0.99$. On the other hand, the early Toarcian interval illustrated slightly heterogeneous OM composition with $r = 0.89$ and variable TOC richness. This indicates rapid changes in the OM productivity and preservation and inputs during the early Toarcian and more stable conditions during the late Bajocian-Bathonian (Fig. 7).

4.1.2 Organic Petrography

The organic petrographic investigation showed that the lower Toarcian interval contains oil-prone marine telalginite and lamalginite (kerogen Type II), primary vitrinite, and solid bitumen (Fig. 8). Alginite particles show a golden-yellow fluorescence, which is consistent with the early phase of oil window (Fig. 8a-b). Other types of

Fig. 4 TOC content versus the petroleum potential ($S_1 + S_2$), indicating the quality of potential source rock intervals



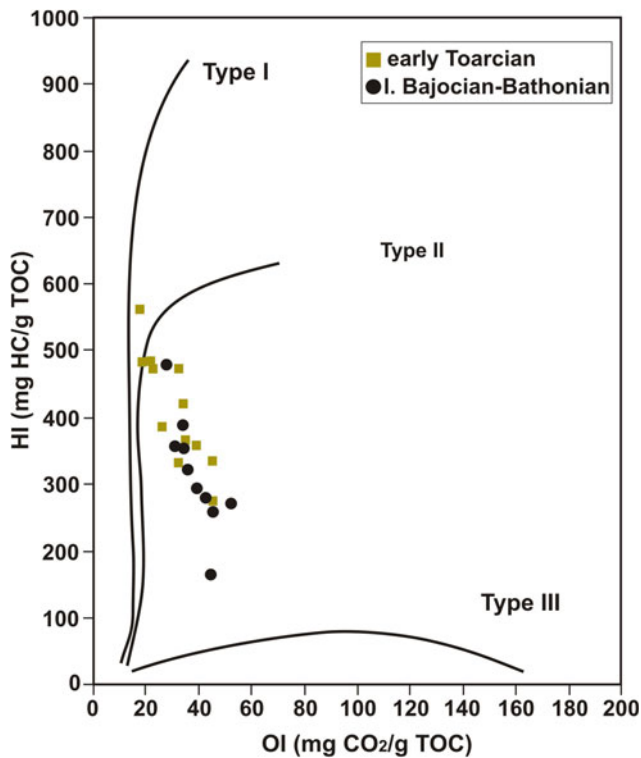


Fig. 5 Modified van Krevelen diagram plot of the studied potential source rock intervals from the upper part of the Quse Formation, Bilong co section

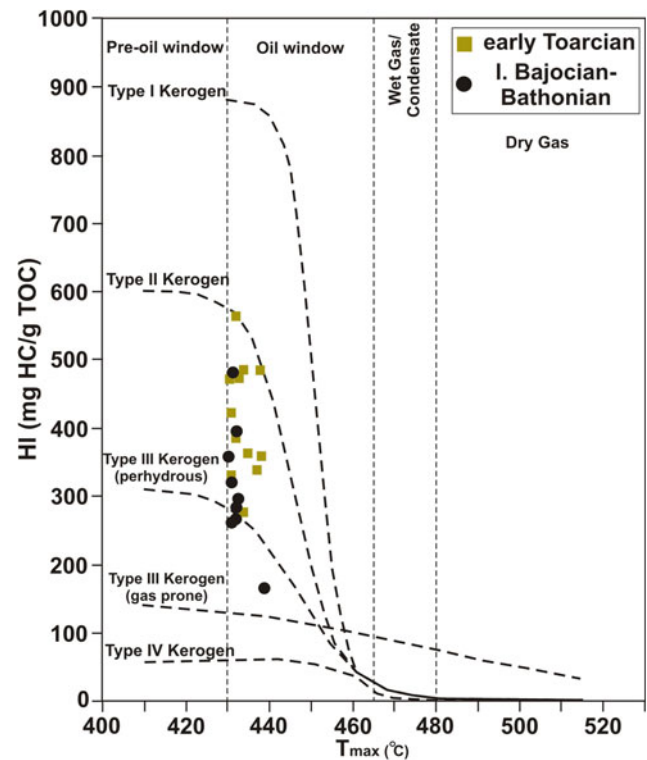


Fig. 7 T_{max} versus HI (sensu Espitalié et al., 1985), discriminating the kerogen types and thermal maturity levels for the upper part of the Quse Formation, Bilong co section

oil-prone liptinites, such as amorphous filamentous algal matter and sporinite exhibit dull olive-green fluorescence (Fig. 8c-d). The upper Bajocian-Bathonian interval shows a similar petrographic composition to the lower section, but low-reflecting vitrinite, primary vitrinite, and inertinite are

more abundant (Fig. 9). The upper interval is rich in paly-nomorphs, especially sphaeromorphs pollen grains, which have dull-yellow fluorescence (Fig. 9b). Faunal inertinite of high maturity setting along with amorphous filamentous algal matter is also present (Fig. 9d, h).

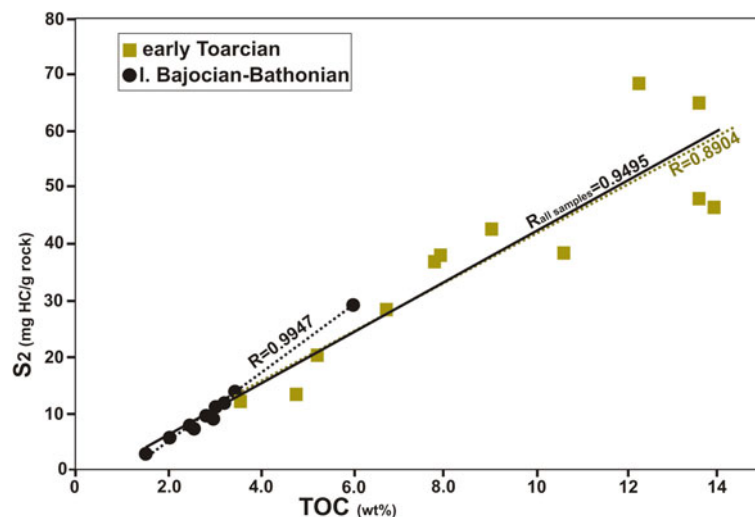


Fig. 6 TOC versus S₂ of the Quse Formation indicates the type of kerogen

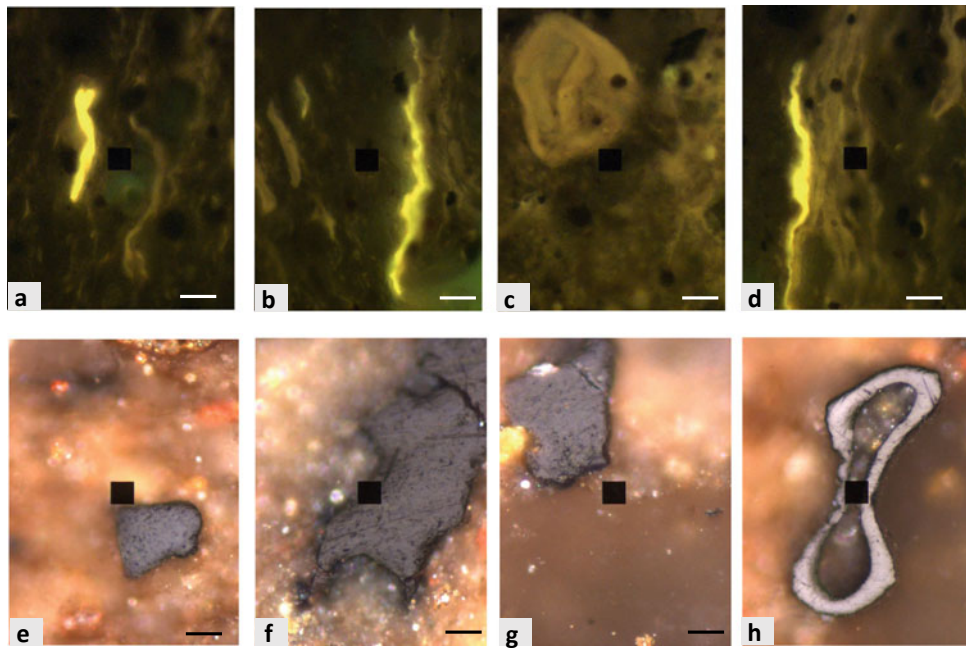


Fig. 8 Photomicrographs of maceral composition for the first group of lower Toarcian samples. **a** BX1-04: Telalginite with golden-yellow fluorescence; **b** BX1-10: Lamalginite with golden-yellow fluorescence; **c** BX1-06: Spherical pollen grains having dull olive-green fluorescence; **d** BX1-06: Amorphous filamentous alginite with dull olive-green fluorescence; **e** BX1-04: Primary vitrinite ($VR_{o,r} = 0.63\%$); **f** BX1-0-1: Angular reservoir bitumen ($VR_{o,r} = 0.59\%$); **g** BX1-07: Primary vitrinite ($VR_{o,r} = 0.66\%$); **h** BX1-07: Inertinite of algal or faunal origin. Photomicrographs A-D were taken under UV light. Excitation is 465 nm, combined dichroic and barrier filter has a cut at 515 nm. The scale bar is 10 μm

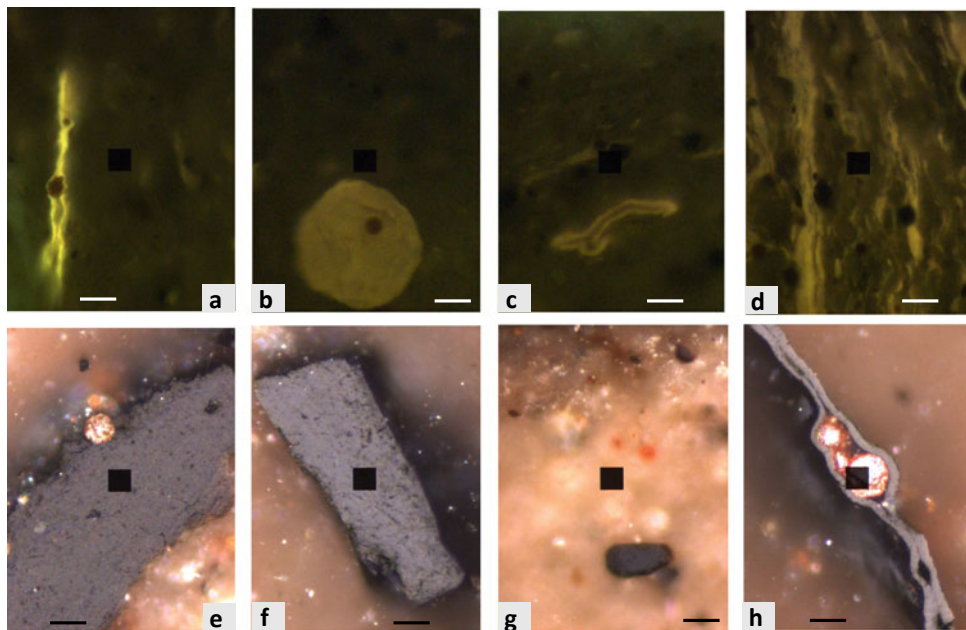


Fig. 9 Photomicrographs of maceral composition for the second group of upper Bajocian-Bathonian samples. **a** BX1-19: Lamalginite with golden-yellow fluorescence; **b** BX1-14: Spherical pollen grains having dull-yellow fluorescence; **c** BX1-30: Compressed spore showing trilete mark and dull-yellow fluorescence; **d** BX1-26: Dull-yellow fluorescing amorphinite; **e** BX1-46: A thick band of low-reflecting vitrinite ($VR_{o,r} = 0.47\%$); **f** BX1-34: A large grain of primary vitrinite ($VR_{o,r} = 0.78\%$); **g** BX1-30: A small grain of primary vitrinite ($VR_{o,r} = 0.73\%$); **h** BX1-46: Inertinite of faunal origin. Photomicrographs a–d were taken under UV light. Excitation is 465 nm, combined dichroic and barrier filter have a cut at 515 nm. The scale bar is 10 μm

4.2 Thermal Maturity Assessment

Evaluating thermal maturity levels of sedimentary OM preserved within the upper Quse and Sewa formations is one of the most important objectives of this study. Organic matter maturation in the studied strata was assessed based on Rock–Eval T_{\max} and random vitrinite reflectance ($VR_{o,r}$); however, due to the scarcity of psilate spores, we could not apply visual maturity evaluation using spore coloration index.

In the Bilong co section, all samples showed comparable T_{\max} values that average 433 °C and similarly relatively low $VR_{o,r}$ values that average 0.69% (Table 1; Fig. 3). PI values are constantly very low and do not exceed 0.07. The foregoing results designate that the OM is early mature. Thermal maturation has also been assessed using the relationship between the HI *versus* T_{\max} (Fig. 7), which further indicates an early maturation stage.

4.3 Palynofacies Analysis

Palynofacies as a term was first defined by Combaz (1964) as the total palynological organic material recovered from kerogen-strewn slides. Furthermore, Traverse (1988) defined it as an assemblage of palynomorphs, signifying local environmental conditions. Palynofacies analysis has been efficiently used in the visual characterization of kerogen types for hydrocarbon potential (Batten & Stead, 2005; Powell et al., 1990; Tyson, 1993, 1995). It has several advantages, which can offer reliable results of kerogen types, whereas its disadvantage is to discriminate hydrogen richness of kerogen (Powell et al., 1990). In many palynological-based kerogen quality assessment studies, AOM-rich kerogen was presumed to correspond to hydrogen-rich OM, thus the relative increase of the AOM content can be considered as an indicator of good source rock potential (Powell et al., 1982). Therefore, AOM is commonly considered a significant proxy when combined with organic geochemical investigations. For that reason, integrating the palynofacies analysis and organic geochemical results underpins the optimal appraisal of possible source rock sediments.

In this study, the particulate organic matter (POM) composition indicates substantial stratigraphic variations in the upper Quse and Sewa formations, which provide an opportunity to distinguish between various palynofacies assemblages and kerogen quality. Preserved POM encompasses both allochthonous particles such as plant pollen and spores, freshwater algae and phytoclasts derived from fluvial/riverine discharge, and autochthonous constituents such as microplanktons, foraminiferal test linings (FTLs), and AOM. Here, we used the AOM-Phytoclasts-Palynomorphs (APP) ternary plot (Tyson, 1993) to elucidate kerogen

types, proximal–distal trends, redox state, as well as relative magnitudes of terrestrial influx.

Within the stratigraphic section, the POM is dominated by moderate to high AOM (36.8–89.2%) *versus* low to moderate phytoclast contents (7–60.6%, Table 1, Fig. 3). The palynomorphs content is generally low and ranges between 0.6 and 19.2% of total content. Only sample BX1-21 exhibits different POM contents. It is composed mainly of palynomorphs of terrestrial origin (53.6%), phytoclasts (43%), and rare AOM content (3.4%, Table 1, Fig. 3). The lower Toarcian interval yielded a moderate recovery of palynomorphs of high degradation compared to high recovery and abundance for the upper Bajocian-Bathonian succession. The recovered palynomorphs from the Quse Formation are mainly terrestrial in origin, including sphaeromorphs pollen compared to low dinoflagellate cysts (dinocysts) and FTLs. Freshwater algae and pteridophyte spores along with marine prasinophytes are rare and comprise a minor percentage of the total palynomorph yield, except for sample BX1-21, which showed a peak of freshwater algae that is represented by *Schizosporis reticulatus*.

Based on the stratigraphic variation of the recovered POM, we defined different kerogen types in the Quse and Sewa formations using palynofacies analysis. The first group of samples, represents the lower Toarcian Quse Formation, plots in the palynofacies fields IX (AOM-dominated) and VI (moderate AOM and phytoclasts) of the APP ternary diagram of Tyson (1993). Fields IX and VI indicate kerogen Type II \geq I and Type II, respectively.

The second group represents the upper Bajocian-Bathonian Sewa Formation and is located mainly in the palynofacies field VIII (AOM-dominated but slightly lower than field IX) of the APP ternary diagram, except for sample BX1-21 that belong to the palynofacies field V (phytoclasts-dominated; Tyson, 1993). Field VIII infers a kerogen Type II \gg I, whereas field V is assigned to kerogen Type III $>$ IV (Tyson, 1993).

4.4 Depositional Environment

The lithologic composition indicates that the Bilong co area contains significant amounts of carbonates mixed with fine siliciclastics. The carbonate content of the investigated samples is in the range of 15.7–46.6% (avg. 32%). The analyzed section is also characterized by high TOC content *versus* low TS values. The relationship between $CaCO_3$ and TOC indicates a shallow marine environment typical of moderate carbonate production, where the organic carbon was negatively correlated with the $CaCO_3$ content ($r = -0.35$, $P < 0.01$, $n = 24$, not shown, e.g., Bohacs et al., 2005; Ricken, 1996). In such an environment, high terrestrial input presumably enhances nutrients, resulting in water

column bioproductivity and high organic carbon accumulation and burial.

The relationship between sulfur and organic carbon is commonly used to differentiate redox levels during deposition, from oxygen-poor anoxia to well-oxygenated settings (Berner, 1984; Leventhal, 1995). Additionally, it provides insights into the activity of microbial sulfate reduction *versus* sulfide oxidation. A strong linear relationship between the former categories reveals a normal marine, oxic setting at the water–sediment interface (Berner, 1984; Leventhal, 1995). The measured total sulfur values (0.98–0.53, avg. 0.78 wt%) are low in these high TOC samples, indicating a moderate relationship between both variables ($r = 0.50$, $P < 0.05$, $n = 6$, not shown). In other words, as TOC changed with time, sulfur content increased slightly, suggesting that sulfur was controlled, to some extent, by the available OM in the water column (Mansour et al., 2020). Relative abundance of oxygen at bottom water settings can also be observed by the Rock–Eval HI and OI cross-plot. For the studied intervals, the high HI *versus* low OI values indicates reduced oxygen contents during deposition (Table 1). Higher values of HI and S_2 compared to moderate TS and organically-bound sulfur reveal better preservation potential of OM probably because of the oxygen-depleted setting at the sea floor (e.g., Mansour et al., 2020).

Furthermore, palynological organic matter is widely used as a reliable proxy indicator of depositional environments under different sedimentary conditions (e.g., Tyson, 1993). Within a sedimentary basin, OM is controlled by some factors that include the type of water column, redox status, sedimentation rates, burial efficiency, proximal–distal trends, and changes in relative sea level (Batten & Stead, 2005; Berner, 1984; Powell et al., 1990; Tyson, 1993). Organic facies can be implemented to characterize the environment of deposition. Besides, palynofacies analysis is a crucial

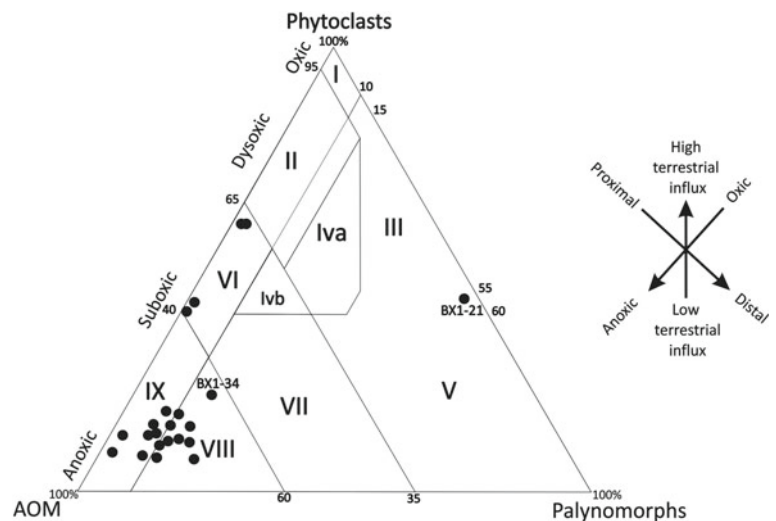
proxy for interpreting depositional environmental settings (Batten, 1996; Tyson, 1993, 1995). Relative changes in POM composition infer oxygenation conditions and thus, can provide a reliable assessment of oxic *versus* anoxic environments. Additionally, POM content is consistent with sea level transgressive–regressive trends and therefore, can provide an estimate of proximal–distal trends from the shoreline (Tyson, 1993, 1995).

In the lower Toarcian Quse Formation in the Bilong co section, most samples are dominated by rich, mixed kerogen associations with rich AOM content *versus* low to moderate content of degraded phytoclasts. Palynomorph composition is characterized by a predominance of terrestrial gymnosperm pollen grains *versus* moderate to low marine dinocysts and rare occurrences of pteridophyte spores, FTLs, freshwater algae, acritarchs, and prasinophytes. This palynofacies assemblage of the studied samples indicates a shallow marine, anoxic to dysoxic shelf environment, whereby sphaeromorphs pollen grains of terrestrial land-plants were transported either by wind action or fluvial input.

Plotting of the retrieved data on the APP ternary diagram indicates that most upper Quse samples are located in field IX, whereas Sewa samples are plotted in field VIII (Fig. 10). These two fields suggest deposition in a distal suboxic-anoxic basin and distal dysoxic shelf settings, respectively, under well-stratified water column distinctive for organic carbon-rich shales (Tyson, 1995). The lowermost oil shale interval (samples BX1-0-7 to BX1-0-3) is characterized by the highest phytoclast content (*ca.* 60.6 to 40% of total POM content, Fig. 11, Table 1), thus suggesting deposition during a high terrestrial input (Fig. 3).

Generally, the relative abundance of AOM is commonly low in marginal to shallow shelf environments and gradually increases in deeper shelf-basinal settings, where enhanced sedimentation, water column stratification, and oxygen

Fig. 10 Plot of samples taken from the upper part of the Quse Formation on the APP ternary diagram of Tyson (1993)



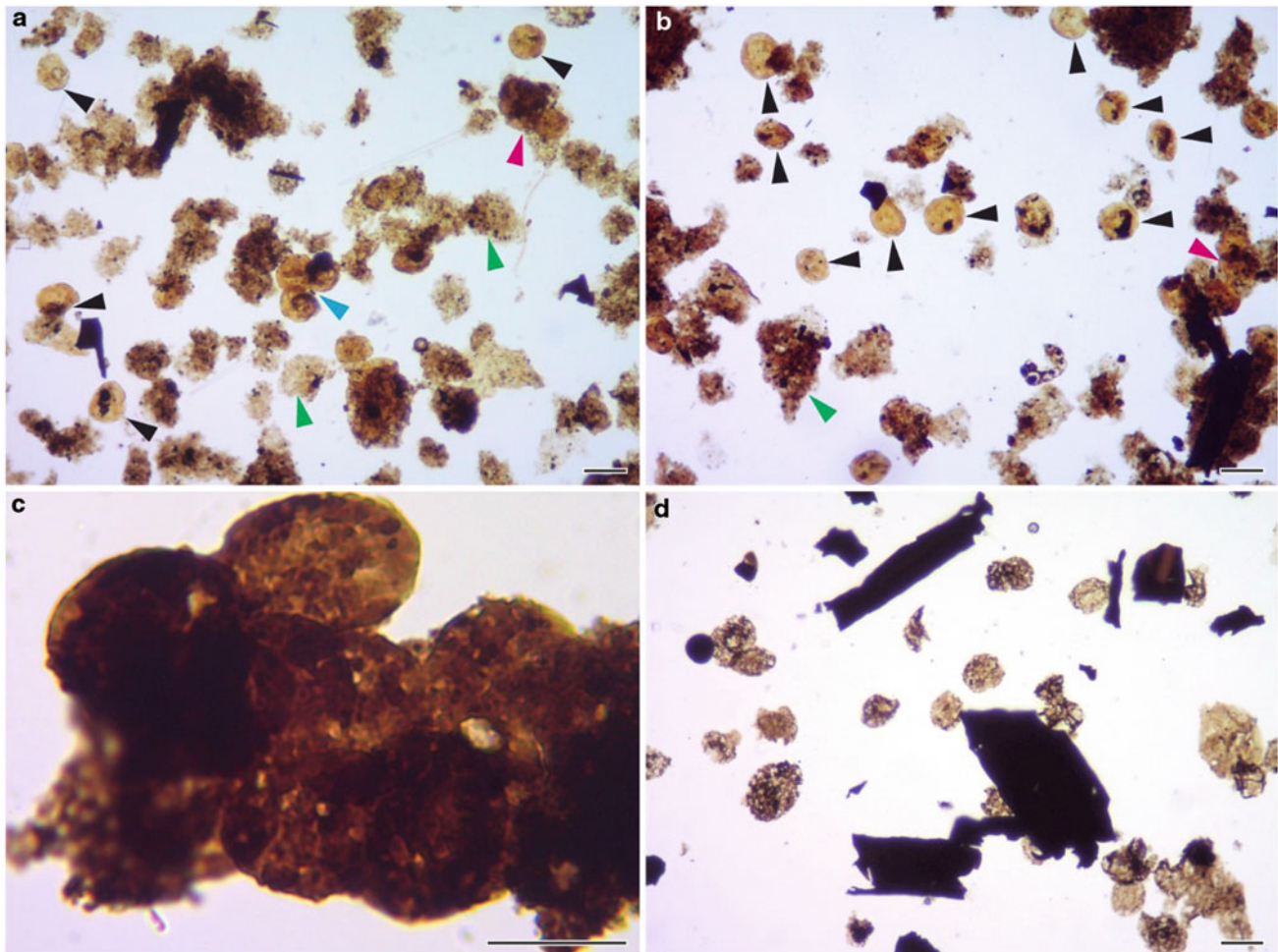


Fig. 11 Transmitted light photomicrographs of POM components from the upper part of the Quse Formation, southern Qiangtang Basin. The scale bar is 40 μm . **a** POM composition of the sample BX1-14 that is dominated by AOM (green arrows) and palynomorphs, mainly sphaeromorphs (black arrows), MFL (pink arrow), *Classopollis* (blue arrow) with low phytoclast content. **b** Palynofacies composition the sample BX1-07 that characterized by AOM richness (green arrows) and sphaeromorphs (black arrows) and low to moderate phytoclasts content. **c** Moderately-preserved sphaeromorphs cluster recovered from the oil shale sample BX1-0-7. **d** Charred or lath-shaped opaque phytoclast and freshwater *Schizosporis reticulatus* algae recovered from the sample BX1-21

depletion allow enhanced preservation of the available organic matter (Mansour et al., 2020; Tyson, 1993, 1995). In most samples of the studied succession, the high proportions of the AOM reveal not only deposition in a marine setting but also reduced oxygen levels and deposition in suboxic to anoxic environment (Fig. 10). This agrees with the existence of pyrite accompanying the AOM in many samples, suggesting the strong impact of microbial mats and enhanced biodegradation under reduced oxygen levels (Pacton et al., 2011).

Sample BX1-21 has a mixed content of palynomorphs (53.6% of total POM) and phytoclasts (43%) compared to very low AOM content (3.4%, Table 1). This sample plots in field V of the APP diagram (Tyson, 1993, Fig. 10), typically of a light-colored bioturbated calcareous mudstone deposited at oxic shelf conditions.

The relative abundance of sphaeromorphs infers a deposition in a basinward direction and in deeper outer neritic shelf environments (Tyson, 1993). For the studied succession, the palynomorphs content is dominated by sphaeromorphs pollen grains that are represented by *Spheripollenites psilatsu*, *Corolina torosa*, *Classopollis* sp., and *Araucariacites australis*, suggesting that the upper Quse and Sewa were deposited in a low-energy, slightly distal inner-neritic environment. The overall scarcity of psilate spores and vascular cryptogamma in the current succession can be attributed to the absence of humid conditions (Abbink, 1998). The overwhelming abundance of the *Classopollis* sp. and *Spheripollenites psilatus* is consistent with many Early Jurassic ecosystems worldwide and was used as a significant indicator of annual dry-arid conditions, allowing the development of coastal forest covers of the

Coniferophyta/Bennetitales and Cheirolepidiaceae that might have grown in the vicinity of the Bilong co (Barrón et al., 2010; Gómez et al., 2008; Mohr, 1989; Slater et al., 2019). An aquatic palynomorph association was represented by low percentages of the above plant families compared to the sphaeromorphs pollen. The association is dominated by peridinioid dinocysts that favor a high nutrient supply in shallow shelf settings, especially in areas of improved terrestrial/riverine input (Brinkhuis, 1994). This interpretation is consistent with the occurrence of freshwater *Schizosporis* algae (Appendix 1), which was triggered by freshwater/riverine supply (Batten, 1996).

Overall, the prevalent environmental circumstances during deposition of the upper interval of the Quse and Sewa formations were mainly anoxic to dysoxic, stagnant distal inner-neritic shelf conditions with a significant contribution of terrestrial/riverine discharge. Only, sample BX1-21 suggests a deposition during high terrestrial input in a shallow marine environment.

Acknowledgements The authors would like to thank the National Natural Science Foundation, China for funding this study (Grant No. 41772105).

References

- Abbink, O. A. (1998). Palynological investigations in the Jurassic of the North Sea region. *Utrecht Laboratory of Palaeobotany and Palynology Contribution Series*, 8, 1–191.
- ASTM D7708-14. (2014). *Standard test method for microscopical determination of the reflectance of vitrinite dispersed in sedimentary rocks*. ASTM International, West Conshohochen, PA. www.astm.org
- Barrón, E., Ureta, S., Goy, A., & Lassaletta, L. (2010). Palynology of the Toarcian-Aalenian global boundary stratotype section and point (GSSP) at Fuentelsaz (Lower–Middle Jurassic, Iberian Range, Spain). *Review of Palaeobotany and Palynology*, 162, 11–28.
- Batten, D. J. (1996). Palynofacies and petroleum potential. In: J. Jansonius, & D. C. McGregor, (Eds.), *Palynology: Principles and applications* (pp. 1065–1084). AASP Foundation.
- Batten, D. J., & Stead, D. T. (2005). Palynofacies analysis and its stratigraphic application. In E. A. M. Koutsoukos (Ed.), *Applied stratigraphy* (pp. 203–226). Springer.
- Behar, F., Beaumont, V., Penteadó, H. L., et al. (2001). Rock-Eval 6 technology: Performances and developments. *Old & Gas Science and Technology Review—IFP*, 56, 111–134.
- Berner, R. A. (1984). Sedimentary pyrite formation: An update. *Geochimica Et Cosmochimica Acta*, 48, 605–615.
- Bohacs, K. M., Grabowski, G. J., & Carroll, A. R. et al. (2005). Production, destruction, and dilution—The many paths to source-rock development (Vol. 82, pp. 61–101). SEPM Special Publication.
- Brinkhuis, H. (1994). Late Eocene to early Oligocene dinoflagellate cysts from the Priabonian type-area (Northeast Italy): Biostratigraphy and paleoenvironmental interpretation. *Palaeogeography, Palaeoclimatology Palaeoecology*, 107(1–2), 121–163.
- Carvajal-Ortiz, H., & Gentzis, T. (2015). Critical considerations when assessing hydrocarbon plays using Rock-Eval pyrolysis and organic petrology data: Data quality revisited. *International Journal of Coal Geology*, 152, 113–122.
- Chen, L., Yi, H. S., Hu, R. Z., et al. (2005). Organic geochemistry of the early Jurassic oil shale from the Shuanghu area in northern Tibet and the early Toarcian oceanic anoxic event. *Acta Geologica Sinica*, 79, 392–397.
- Chen, L., Mattioli, E., Da, X. J., et al. (2018). Calcareous nannofossils from the Jurassic black shales in the Qiangtang Basin, northern Tibet (China): New records of stratigraphic ages and palaeoceanography. *Newsletters on Stratigraphy*, 52(1), 55–72.
- Combaz, A. (1964). Les Palynofacies. *Review Micropaleontology*, 7, 205–218.
- Ding, L., Yang, D., Cai, F., et al. (2013). Provenance analysis of the Mesozoic Hoh-Xil-Songpan-Ganzi turbidites in northern Tibet: Implications for the tectonic evolution of the eastern Paleo-Tethys Ocean. *Tectonics*, 32, 34–48.
- Espitalié, J., Deroo, G., & Marquis, F. (1985). La pyrolyse Rock-Eval et ses applications (Vol. 40, pp. 563–579). Partie 1. Revue Institute Francais Petrole.
- Fang, X., Song, C., Yan, M., et al. (2016). Mesozoic litho- and magneto-stratigraphic evidence from the central Tibetan Plateau for megamonsoon evolution and potential evaporites. *Gondwana Research*, 37, 110–129.
- Fu, X., Tan, F., Feng, X., et al. (2014). Early Jurassic anoxic conditions and organic accumulation in the eastern Tethys. *International Geology Review*, 56(12), 1450–1465.
- Fu, X., Wang, J., Zeng, S., et al. (2017). Continental weathering and palaeoclimatic changes through the onset of the Early Toarcian oceanic anoxic event in the Qiangtang Basin, eastern Tethys. *Palaeogeography, Palaeoclimatology, Palaeoecology*, 487, 241–250.
- Gómez, J. J., Goy, A., & Canales, M. L. (2008). Seawater temperature and carbon isotope variations in belemnites linked to mass extinction during the Toarcian (Early Jurassic) in central and northern Spain, Comparison with other European sections. *Palaeogeography, Palaeoclimatology, Palaeoecology*, 258, 28–58.
- ISO 7404-2. (2009). *Methods for the petrographic analysis of coal—Part 2: Methods of preparing coal samples*. International Organization for Standardization. ISO 7404-2:2009(en). www.iso.org/standard/42798.html
- ISO 7404-5. (2009). *Methods for the petrographic analysis of coal—Part 5: Methods of determining microscopically the reflectance of vitrinite* (p. 14). International Organization for Standardization, Geneva, Switzerland.
- Jenkyns, H. C. (2010). Geochemistry of oceanic anoxic events. *Geochemistry, Geophysics, Geosystems*, 11, Q03004.
- Ji, C. J., Xia, G. Q., Yi, H. S., et al. (2014). Aromatic hydrocarbons in the Biluo Co oil shale of the Shuanghu area, northern Tibetan Plateau, and their implications. *Oil Shale*, 31(4), 351–364.
- Kapp, P., DeCelles, P. G., Gehrels, G. E., et al. (2007). Geological records of the Lhasa-Qiangtang and Indo-Asian collisions in the Nima area of central Tibet. *Geological Society of America Bulletin*, 119, 917–932.
- Lamoureux-Var, V., Espitalié, J., & Pillot, D., et al. (2019). Rock-Eval 7S: Technology and performance. In: *29th International Meeting of Organic Geochemistry* (Vol. 1, pp. 1–2). European Association of Geoscientists and Engineers.
- Leventhal, J. S. (1995). Carbon-sulfur plots to show diagenetic and epigenetic sulfidation in sediments. *Geochimica Et Cosmochimica Acta*, 59, 1207–1211.
- Li, Y., Wang, C. S., & Yin, H. S. (2002). Filled sequence and evolution of the Mesozoic Qiangtang composite foreland basin in the Qianghai-Tibet Plateau. *Journal of Strategy*, 26, 62–79. (in Chinese with English abstract).
- Li, G. J. (2016). *Research on sedimentary facies and hydrocarbon source rocks of upper Triassic and Lower to Middle Jurassic in the*

- South Qiangtang depression, Tibet (pp. 1–85). Master Thesis, Chengdu: Chengdu University of Technology (in Chinese with English abstract).
- Ma, A. L., Hu, X. M., Garzanti, E., et al. (2017). Sedimentary and tectonic evolution of the southern Qiangtang basin: Implications for the Lhasa-Qiangtang collision timing. *Journal of Geophysical Research: Solid Earth*, 122, 4790–4813.
- Mansour, A., Gentzis, T., & Carvajal-Ortiz, H., et al. (2020). Geochemistry and palynology of the upper Albian at the Abu Gharadig Basin, southern Tethys: Constraints on the oceanic anoxic event 1d. *Geological Journal*, 55(9), 6338–6360. <https://doi.org/10.1002/gj.3810>
- Mohr, B. A. R. (1989). New palynological information on the age and environment of Late Jurassic and Early Cretaceous vertebrate localities of the Iberian Peninsula (eastern Spain and Portugal). *Berl Geowiss Abh Reihe A*, 106, 291–301.
- Pacton, M., Gorin, G. E., & Vasconcelos, C. (2011). Amorphous organic matter—experimental data on formation and the role of microbes. *Review of Palaeobotany and Palynology*, 166, 253–267.
- Peters, K. E. (1986). Guidelines for evaluating petroleum source rock using programmed pyrolysis. *AAPG Bulletin*, 70, 318–329.
- Peters, K. E., & Cassa, M. R. (1994). Applied source rock geochemistry. In: L. B. Magoon, & W. G. Dow (Eds.), *The petroleum system—From source to trap*. AAPG Memoir, Vol. 60, pp. 93–120.
- Powell, T. G., Creaney, S., & Snowdon, L. R. (1982). Limited use of organic petrographic techniques for identification of petroleum source rocks. *AAPG Bulletin*, 66, 430–435.
- Powell, A. J., Dodge, J. D., Lewis, J. (1990). Late Neogene to Pleistocene palynological facies of the Peruvian continental margin upwelling, Leg 112. In: E. Suess, R. Von Huene (Eds.), *Proceeding of the ocean drilling project, scientific results* (Vol. 112, pp. 297–321). ODP, College Station, Texas.
- Ricken, W. (1996). Bedding rhythms and cyclic sequences as documented in organic carbon-carbonate patterns, Upper Cretaceous, Western Interior, U.S. *Sedimentary Geology*, 102, 131–154.
- Rullkötter, J., Leythaeuser, D., Horsfield, B., et al. (1988). Organic matter maturation under the influence of a deep intrusive heat source: A natural experiment for quantitation of hydrocarbon generation and expulsion from a petroleum source rock (Toarcian shale, northern Germany). *Organic Geochemistry*, 13, 847–856.
- Sengör, A. M. C. (1987). Tectonics of the Tethysides: Orogenic collage development in a collisional setting. *Annual Review of Earth and Planetary Science*, 15, 213–244.
- Slater, S. M., Twitchett, R. J., Danise, S., et al. (2019). Substantial vegetation response to Early Jurassic global warming with impacts on oceanic anoxia. *Nature Geoscience*, 12, 462–467.
- Su, X., Yin, Y. R., Zhu, Y. H., et al. (2015). Late early Jurassic Posidonia shale facies in Qiangtang Basin and its chronostratigraphic significance. *Geological Bulletin of China*, 34, 1617–1628. (in Chinese with English abstract).
- Traverse, A. (1988). *Paleopalynology* (p. 600). Unwin Hyman.
- Tyson, R. V. (1993). Palynofacies analysis. In D. G. Jenkins (Ed.), *Applied micropaleontology* (pp. 153–191). Kluwer Academic Publication.
- Tyson, R. V. (1995). *Sedimentary organic matter-organic facies and palynofacies* (p. 615). Chapman and Hall.
- Wang, C. S., Chang, E. Z., & Zhang, S.-N. (1997). Potential oil and gas-bearing basins of the Qinghai-Tibetan plateau, China. *International Geology Review*, 39(10), 876–890.
- Wang, C. S., Yi, H. S., Liu, C. Y., et al. (2004). Discovery of paleo-oil-reservoir in Qiangtang Basin in Tibet and its geological significance. *Oil and Gas Geology*, 25(2), 139–143. [in Chinese with English abstract].
- Wang, Y. S., Zhang, S. Q., Xie, Y. H., et al. (2012). *1:250000 regional geological survey report of the People's Republic of China (Angdarco Sheet)*. Publishing House of China University of Geosciences.
- Wang, C. S., Dai, J. G., Zhao, X. X., et al. (2014). Outward-growth of the Tibetan Plateau during the Cenozoic: A review. *Tectonophysics*, 621, 1–43.
- Wang, Z., Wang, J., Fu, X., et al. (2019). Sedimentary successions and onset of the Mesozoic Qiangtang rift basin (Northern Tibet), southwest China: Insights on the Paleo- and Meso-Tethys evolution. *Marine and Petroleum Geology*, 102, 657–679.
- Wood, G. D., Gabriel, A. M., Lawson, J. C. (1996). Chapter 3. Palynological techniques-processing and microscopy. In: J. Jansoni, & D. C. McGregor (Eds.), *Palynology: Principles and applications* (Vol. 1, pp. 29–50). AASP Foundation.
- Xia, G., Ji, C., Chen, L., et al. (2017). Biomarkers of the Lower Jurassic black shale in the Shuanghu area of the Qiangtang Basin, Northern Tibet, and their geological significance. *Oil Shale*, 34(1), 55–69.
- Yao, H. Z., Zhang, R. J., Duan, Q. F., et al. (2011). Jurassic rocks, bivalves, and depositional environments of the source area of the Yangtze River, Qinghai Province, western China. *Science China Earth Sciences*, 54, 1136–1148.
- Yi, H. S., Lin, J. H., Zhao, B., et al. (2003). New biostratigraphic data of the Qiangtang area in the northern Tibetan plateau. *Geology Review*, 49, 59–65. [In Chinese with English abstract].
- Yi, H. S., Wang, C. S., Lin, J. H., Shi, Z. Q., Chen, L., Wu, X. H., Wei, Q. L., Zhang, X. Q. (2005). Jurassic ammonite fauna in the Amdo area, northern Tibet and its paleogeographic implications. *Geological Bulletin of China*, 24(1), 41–47 (in Chinese with English abstract).
- Yi, H. S., Chen, L., Jenkyns, H., et al. (2013). The Early Jurassic oil shales in the Qiangtang Basin, northern Tibet: Biomarkers and Toarcian oceanic anoxic events. *Oil Shale*, 30, 441–455.
- Yin, A., & Harrison, T. M. (2000). Geologic evolution of the Himalayan-Tibetan orogen. *Annual Review of Earth and Planetary Sciences*, 28, 211–280.
- Yin, J., & Chandler, R. B. (2016). Aalenian to Lower Bajocian ammonites from the Qiangtang block (North Tibet). *Proceedings of the Geologists' Association*, 127, 172–188.
- Zhu, D. C., Zhao, Z. D., Niu, Y. L., et al. (2013). The origin and pre-Cenozoic evolution of the Tibetan Plateau. *Gondwana Research*, 23, 1429–1454.